OPEN

Correspondence and
requests for materials
should be addressed to
H.L. (nilnish@gmail.
com)

Thickness dependence of spin polarization and electronic structure of ultra-thin films of MoS$_2$ and related transition-metal dichalcogenides

Tay-Rong Chang[1], Hsin Lin[2], Horng-Tay Jeng[1,4] & A. Bansil[3]

[1]Department of Physics, National Tsing Hua University, Hsinchu 30013, Taiwan, [2]Graphene Research Centre and Department of Physics, National University of Singapore, Singapore 117542, [3]Department of Physics, Northeastern University, Boston, Massachusetts 02115, USA, [4]Institute of Physics, Academia Sinica, Taipei 11529, Taiwan.

We have carried out thickness dependent first-principles electronic structure calculations on ultra-thin films of transition-metal dichalcogenides MX$_2$ (M=Mo or W; X=S, Se, or Te). When spin-orbit coupling (SOC) is included in the computations, monolayer MX$_2$ thin films display spin-split states around the valence band maximum at the Brillouin zone corners with nearly 100% spin polarization. The spins are aligned oppositely along out-of-the-plane direction at the K and K′ points. For the bilayer films, spin polarization of this SOC induced band splitting can be switched on or off by an out-of-the-plane external electric field. The spin-polarized states are weakly coupled between the layers in bulk MX$_2$ compounds with small k_z dispersion. We confirm a transition from an indirect to direct band gap as the thickness is reduced to a monolayer in MoS$_2$, in agreement with recent experimental findings. Owing to the presence of a large spin-splitting energy and an insulating band gap, MX$_2$ compounds have great potential for spin/valley electronic applications at room temperature.

Two-dimensional (2D) materials have been drawing increasing attention because of their potential applications in next generation electronics. Graphene[1], which is currently the most widely investigated 2D material, possesses high mobility[2] and displays rich physics[3–5] driven by the presence of Dirac cone dispersions near the Fermi level at K and K′ points at the Brillouin zone corners[6]. However, graphene is a gapless system and the spin on the Dirac cone is a pseudospin, limiting its usefulness in semiconductor industry or spintronics device technologies. For these reasons, it is clearly important to find new 2D materials, which contain not only a large band gap but also support spin-polarized states.

A number of 2D materials with spin-polarized states have been synthesized. These include, HgTe quantum wells and related systems[7,8], silicene[9], and transition-metal dichalcogenide (MX$_2$) family[10–12]. While HgTe quantum well systems and free-standing silicene and related compounds are predicted to be 2D quantum spin Hall (QSH) insulators with small band gaps[13–15], MX$_2$ family harbors much larger band gaps, and a monolayer MoS$_2$ transistor has been reported recently[16]. Radisavljevic et al. used a hafnium oxide gate dielectric to demonstrate a room-temperature monolayer MoS$_2$ mobility of at least 200 cm^2 V^{-1} s^{-1} [16]. In monolayer MoS$_2$, both the valence and conduction band extremes are located at the corners (K-points) of the 2D hexagonal Brillouin zone[17–19], resulting in two inequivalent valleys for low energy carriers which are similar to graphene. Bulk MoS$_2$ has been demonstrated with a large indirect gap, while its monolayer thin-film exhibits a direct band gap[20,21]. Unlike graphene, monolayer MoS$_2$ lacks spatial inversion symmetry and has a strong spin-orbit coupling (SOC) originating from the d orbitals of the heavy transition-metal atoms[19]. It has been shown that due to the presence of a large direct band gap, inversion symmetry breaking, and a strong SOC, optical pumping with circularly polarized light can achieve a valley polarization of 30% in pristine monolayer MoS$_2$[22,23]. In order to achieve continuous and reversible control of valley-contrasting properties, Wu et al. investigated bilayer MoS$_2$ by using polarization-resolved photoluminescence[24]. In bilayer MoS$_2$ the circularly polarized photoluminescence can be continuously tuned from −15% to 15% as a function of gate voltage, whereas in structurally non-centrosymmetric monolayer MoS$_2$ the photoluminescence polarization is gate independent[24]. Recently, Cheng et al. have demonstrated that monolayer MoS$_2$ is a 2D diluted magnetic semiconductor[25] in which valley polarization can be

induced and controlled by magnetic doping[26]. They have also investigated the interlayer coupling in ultra thin MoS_2[27] and the Rashba effect in MXY (M = Mo, W and X, Y = S, Se, Te) compounds[28]. A field-dependent unconventional Hall plateau sequence[29] is predicted theoretically in trilayer MoS_2, and multilayer MoS_2 has been shown to be a superconductor at optimal doping[30].

Motivated by the intense current interest in 2D transition-metal dichalcogenides, the present work undertakes a comprehensive first-principles investigation of ultra-thin films of these materials, and systematically analyzes their spin-polarization characteristics and how these evolve with film thickness, and delineates how different chalcogens in Mo and W based films modify their electronic structures. When the SOC is included in the computations, band structures display spin-split valence bands around the K-points for monolayer MX_2 thin-films which do not possess inversion symmetry. The spin of the top valence states is found to be aligned along out-of-the-plane direction with the spin pointing up at the K-point and down at the K′-point. The inversion symmetry is restored in bilayer thin films. Here, we find that when an out-of-the-plane electric field E_z is applied, the inversion symmetry is removed and the spin degeneracy at the K-point is lifted. The spin-splitting energy increases with increasing E_z and saturates for E_z larger than a critical field E_c. In the high temperature limit, spin polarization for slabs with even number of layers is zero, while slabs with odd number of layers obey $1/x$ decay with increasing film thickness x. Finally, we show that the position of the valence band maximum shifts from the K-point to the Γ point as the film thickness increases. In particular, we confirm a transition from an indirect to a direct band gap as the thickness is reduced to a monolayer in MoS_2, in agreement with recent experimental findings[20,21].

Computational Details

MX_2 compounds crystallize in a layered 2H prototype structure with space group $P6_3/mmc$ (Fig. 1), which contains two inverse MX_2 layers. In each layer, intermediate M atom is sandwiched between X atoms, forming strong ionic bonds within a trigonal local structure (Fig. 1 (b)). While the intralayer M-X bonding is strong, the interlayer bonding is weak as it arises from van der Waals forces (Fig. 1 (c)). Unlike the bulk crystal, the space group of monolayer MX_2 is not $P6_3/mmc$ but reduces to $P\bar{6}m2$ due to loss of inversion symmetry. The inversion symmetry is restored in bilayer thin films: In Fig. 1, we used MoS_2 as an example where the inversion center is marked by red dot in Fig. 1 (c) lies between two adjacent MoS_2 layers.

The electronic structures of MX_2 films were computed using the projector augmented wave method[31,32] as implemented in the VASP[33–35] package within the generalized gradient approximation (GGA)[36] scheme. The SOC effects were included in a self-consistent manner. Slabs with vacuum thickness larger than 15 Å were used to model the thin films. A 15 × 15 × 1 Monkhorst-Pack k-point mesh was used in the computations. The experimental lattice constants were used[10,37,38]. Note that although experimental lattice constants are available for all six compounds studied, the experimental atomic positions are not available for all these compounds. In order to meaningfully unfold trends in electronic structures as a function of the number of layers or strain, it is important of course to use a consistent theoretical framework in computations. Accordingly, relaxed theoretical atomic positions were systematically used in making such comparisons. The atomic positions were relaxed until the residual forces were less than 0.005 eV/Å.

Results and Discussion

Fig. 1 (d) shows the electronic band structure of monolayer MoS_2. Without SOC (red dashed line), a direct band gap of ∼1.6 eV is obtained between the valence band maximum and conduction band minimum at the K-point, and all bands are found to be spin degenerate. When the SOC is turned on (black line), the top valence bands
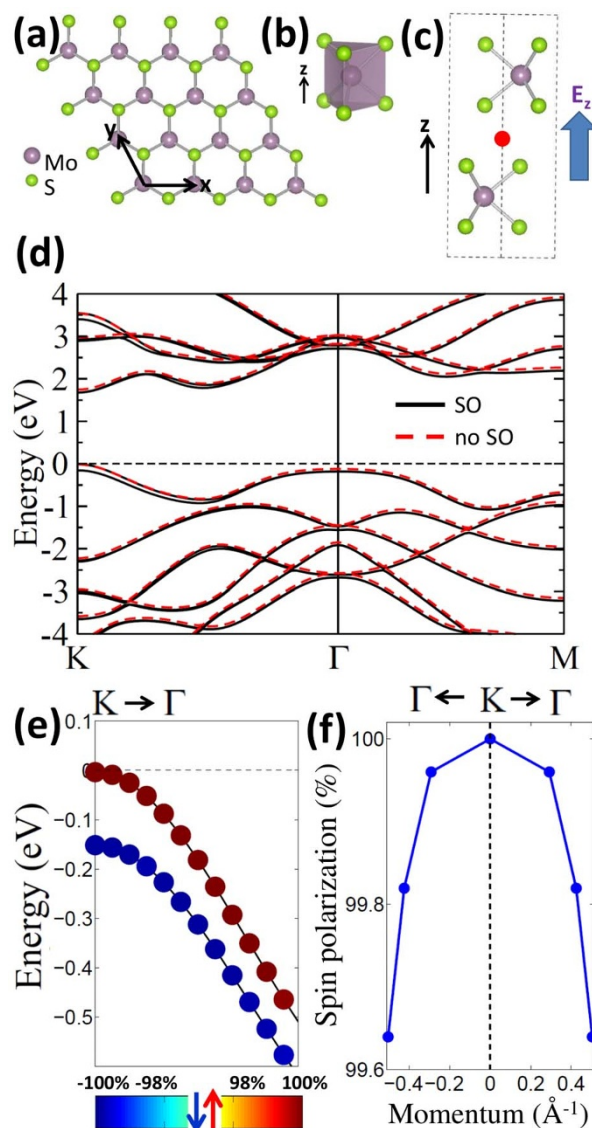

Figure 1 | (a) Top view of a monolayer MoS_2 thin-film. Gray and yellow dots denote Mo and S atom, respectively. (b) Trigonal local structure of MoS_2. (c) Side view of bilayer structure of a MoS_2 thin-film. Red dot marks the spatial inversion symmetry point. (d) Band structure of a MoS_2 monolayer. Black and red dashed lines give results with and without SOC, respectively. (e) Spin polarization near the K-point around E_F. Color bar denotes strength of spin polarization. (f) Spin decay behavior of polarization strength near the K-point.

display a significant splitting (∼ 150 meV) at the K-point due to the breaking of spatial inversion symmetry ($E(k,\uparrow) = E(-k,\uparrow)$). In sharp contrast, the top valence bands are spin degenerate at the Γ and M points. This is because Γ and M points are time-reversal invariant while K-point is not. Focusing on the split band, we find that it displays nearly 100% out-of-the-plane spin polarization (Fig. 1 (e)), which is consistent with previous results[19,39,40]. The two bands at K and K′ have opposite spin polarizations, obeying the constraint of time reversal symmetry ($E(k,\uparrow) = E(-k,\downarrow)$). Fig. 1 (f) shows the degree of spin polarization for the top valence band near the K- point. The bands are nearly 100% spin polarized at the K-point, and decay very little as the momentum deviates from the K-point within 0.5 Å^{-1}.

We emphasize that the presence of a robust 100% spin-polarized band at the top of valence bands in an MX_2 monolayer results from symmetry constraints of mirror symmetry[40] and the broken inver-

sion symmetry of the underlying crystal structure, and therefore, this polarization cannot be switched off by an external field. In this connection, we have investigated MX_2 bilayers in which the inversion symmetry is restored with a center of inversion in the structure lying between the two layers in the bilayer. Fig. 2(a) shows the band structure of a MoS_2 bilayer. Since the inversion symmetry is now restored, all bands are spin-degenerate. The energy difference between the top of the valence bands at the K and Γ points, $\Delta_{K\Gamma}$, becomes smaller. Notably, the splitting at the Γ point is due to the interaction between the two MX_2 layers, but the SOC is responsible for the splitting at the K-points [Fig. 2(b)].

The inversion symmetry of bilayer MX_2 can, however, be removed by an out-of-the-plane external field, E_z, which lifts the spin degeneracy of states away from the time-reversal-invariant points in the Brillouin zone. Since K-points are not time-reversal-invariant points, the spin-splitting at the top of the valence bands can be manipulated via E_z. Fig. 2(b) shows how the bilayer MoS_2 band structure evolves with increasing E_z. For non-zero E_z, there are four spin-polarized states in a bilayer, two of which come from the first layer and the other two from the second layer in the bilayer system. We define the interlayer splitting energy, Δ_{inter}, to be the energy difference between the first-layer spin-up state and the second layer spin-down state. We also define the intralayer splitting energy, Δ_{intra}, to be the energy difference between the first-(second-)layer spin-up state and the first-(second-)layer spin-down state. At $E_z = 0.1$ eV/Å, the states from the second layer are slightly lower than those from the first layer in each split branch, making Δ_{inter} less than Δ_{intra}, in agreement with previous results[41–43]. [The two topmost valence states are from different layers.] When E_z is larger than a critical value E_c, Δ_{inter} becomes larger than Δ_{intra}, making the two topmost valence states to come from the same layer. Fig. 2 (c) shows Δ_{inter} and Δ_{intra} as a function of E_z. We see that Δ_{inter} increases linearly as E_z increases, but Δ_{intra} remains nearly constant. Δ_{inter} is due to the potential difference between two layers caused by E_z. On the other hand, Δ_{intra} is the spin-

splitting resulting from the effect of SOC within each layer, and it therefore depends weakly on E_z. There is a crossover between Δ_{inter} and Δ_{intra} for $0.1 < E_z < 0.2$. This indicates that the maximum of the spin-splitting energy is about 150 meV (solid line in Fig 2(c)), which is comparable to the intrinsic value of the monolayer spin-splitting (Δ_{intra}). Δ_{inter} under high E_z ($E_z > E_c$), red dashed line in Fig 2(c), is not relevant to the spin-splitting at the two topmost valence bands, both of which now primarily come from the same layer. Note that the main effect of E_z is to induce a significant band-splitting with little change in the degree of spin polarization. The spin direction reverses when the direction of the E_z reverses, providing an effective pathway for manipulating spin states. These spin-polarized states could be observed via spin sensitive angle-resolved photoemission experiments, important matrix element effects in ARPES and other highly resolved spectroscopies[44] notwithstanding, and should be accessible to transport experiments in hole-doped samples.

Figure 3(b) shows the band structure of bulk MoS_2 at selected k_z values. The two well-separated branches can still be seen at the K point because the SOC induced splitting is much larger than the k_z dispersion resulting from interlayer coupling. The SOC splitting is about 150 meV, which is comparable to the value of Δ_{intra} in the bilayer or the spin-splitting energy in the monolayer, while the interlayer coupling at the K-point is estimated to be only about 25 meV. Note that when the number of layers is finite, the number of states in each branch is the same as the number of MX_2 layers.

Concerning the spin-polarization for the top branch of the valence bands at the K-point, it is interesting to consider the degree of spin polarization in the high temperature limit when states in the top branch will become accessible due to thermal fluctuations. Since a multilayer with an even number of layers is inversion symmetric, there will be no net spin polarization in a branch containing an even number of states. Adding one MX_2 layer to create a multilayer with an odd number of layers, however, adds a fully spin polarized state
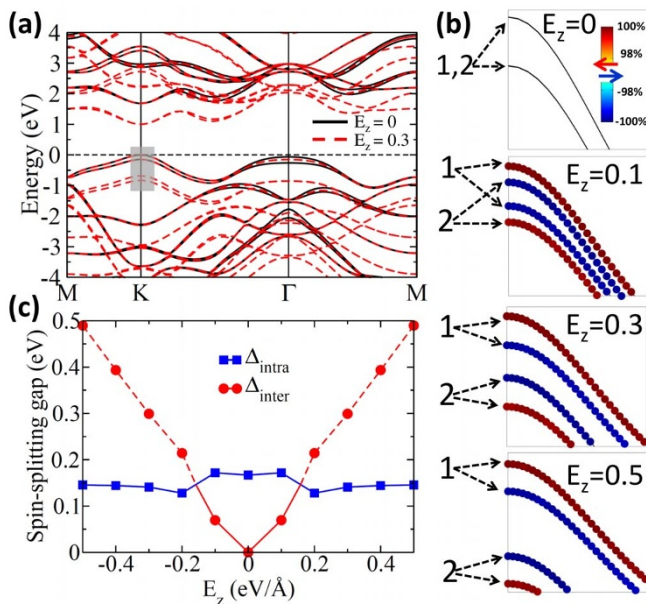

Figure 2 | (a) Band structure of bilayer MoS_2. Black and red dashed lines give results at $E_z = 0$ and $E_z = 0.3$ (eV/Å), respectively. (b) Evolution of band structure near the K-point (red dashed box in Fig. 2(a)) for varying external electric field, E_z. Color scale gives the degree of spin polarization. Contributions from the first and second layers in MoS_2 bilayer are marked with numbers 1 and 2. The unit of electric field is eV/Å. (c) Spin-splitting energy at the K-point as a function of E_z. Blue line gives the intralayer splitting energy, Δ_{intra}, While the red line gives the interlayer splitting, Δ_{inter}.
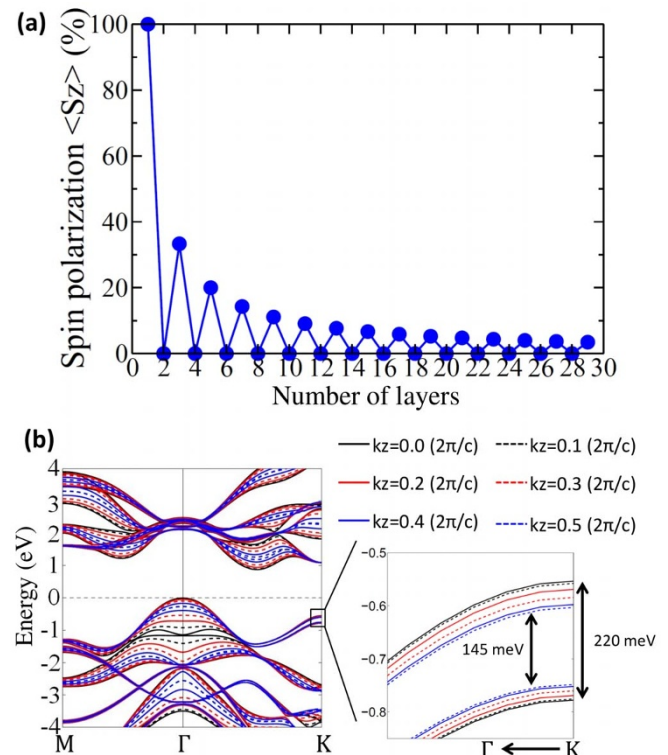

Figure 3 | (a) Average spin polarization of the top branch of valence bands as a function of the number of MX_2 layers. (b) Band structure of bulk MoS_2 at selected k_z values (in unit of $2\pi/c$). Solid and dashed lines of various colors refer to different k_z values (see legend).

into the branch. Despite the mixing of other states through the weak interlayer coupling, the average out-of-the-plane spin polarization for the whole branch becomes nonzero. The degree of spin polarization for the top branch is inversely proportional to the number of layer, x. As shown in Fig. 3(a), the average spin polarization, $<S_z>$, of the top branch at the K-point as a function of thickness in the high temperature limit can be expressed as

$$f(x) = \begin{cases} 0 & x = 2,4,6\ldots \\ 1/x & x = 1,3,5\ldots \end{cases}$$

Note that the states at K′ possess opposite spin polarization. Therefore, f(x) will take minus sign for the top branch at K′.

We comment further on the nature of valence bands at the Γ point. Unlike the K-point, since Γ is a time-reversal-invariant point, states at Γ are spin degenerate for any number of layers. With increasing number of layers, as more states interact through interlayer coupling, the bandwidth increases, and the top of the valence band at Γ moves to higher energy. In MoS_2, the interlayer coupling at Γ is ~0.25 eV, an order of magnitude larger than that for top valence states at the K-point. This drastic difference in the strength of interlayer coupling is due to the orbital character of the relevant states: The top valence states at Γ are primarily associated with out-of-the-plane $d_{3z^2-r^2}$ orbital, while states at the K-points arise from in-plane d_{xy} and $d_{x^2-y^2}$ orbitals.

Accessibility of spin polarized valence states for spintronics applications will be controlled by the size of SOC spin-splitting energy Δ_{intra} and the energy difference between the top valence states at K and Γ, $\Delta_{K\Gamma} = E_K - E_\Gamma$. Accordingly, Fig. 4(a) compares these key quantities in various MX_2 materials. Δ_{intra} is seen to increase with increasing atomic number as expected since the strength of SOC is larger in heavier atoms. $\Delta_{K\Gamma}$, on the other hand, does not show any simple trend. Interestingly, the value of $\Delta_{K\Gamma}$ correlates with that of X-M-X bond angle (solid green line). This indicates that the crystal field and M-X bonding, which determine the relative positions of various orbitals, also play an important role in determining $\Delta_{K\Gamma}$.

In order to help guide search for suitable substrates, we have explored the effect of strain on Δ_{intra} and $\Delta_{K\Gamma}$. Fig. 4(b) shows $\Delta_{K\Gamma}$ as function of strain for monolayer, bilayer, and bulk MoS_2. $\Delta_{K\Gamma}$ is seen to increase (decrease) as the lattice constant decreases (increases). This trend is consistent with our observation above that $\Delta_{K\Gamma}$ correlates with the X-M-X bond angle in that thin films with larger in-plane lattice constant possess smaller X-M-X bond angles. Interestingly, $\Delta_{K\Gamma}$ is very small for bilayer MoS_2, and only a 1% lattice constant increase changes its sign, adding to the possibilities for control of spin-polarized states via an external electric field. Notably, the small value of $\Delta_{K\Gamma}$ in bilayer can change sign if experimental atomic positions are used in the computations instead of self-consistently optimized theoretical positions[41–43]. This discrepancy between experiment and theory is due to overestimation of the bond-length and bond-angle in GGA, which is a typical error of the GGA exchange-correlation functional[45]. Despite these uncertainties in absolute band positions, the trends shown are fairly robust to whether theoretical or experimental atomic positions are used consistently in the calculations. We suggest that substrates should be chosen with smaller lattice constants so as to have larger $\Delta_{K\Gamma}$ values. Note also that unlike $\Delta_{K\Gamma}$, which is sensitive to in-plane strain and slab thickness, Δ_{intra} is found to be almost constant (not shown) when strain, E_z, or thickness is varied.

Concerning the nature of the band gap and whether it is direct or indirect, we note that all MX_2 considered here have valence band maximum at Γ for bulk and at K for monolayer. Take MoS_2 as an example. Fig. 4(c) shows that $\Delta_{K\Gamma}$ decreases as slab thickness increases. As shown in Fig. 3(b), the valence band maximum is at Γ and conduction band minimum is away from Γ along the Γ-K direction, so that the bulk band gap is indirect. For monolayer MoS_2
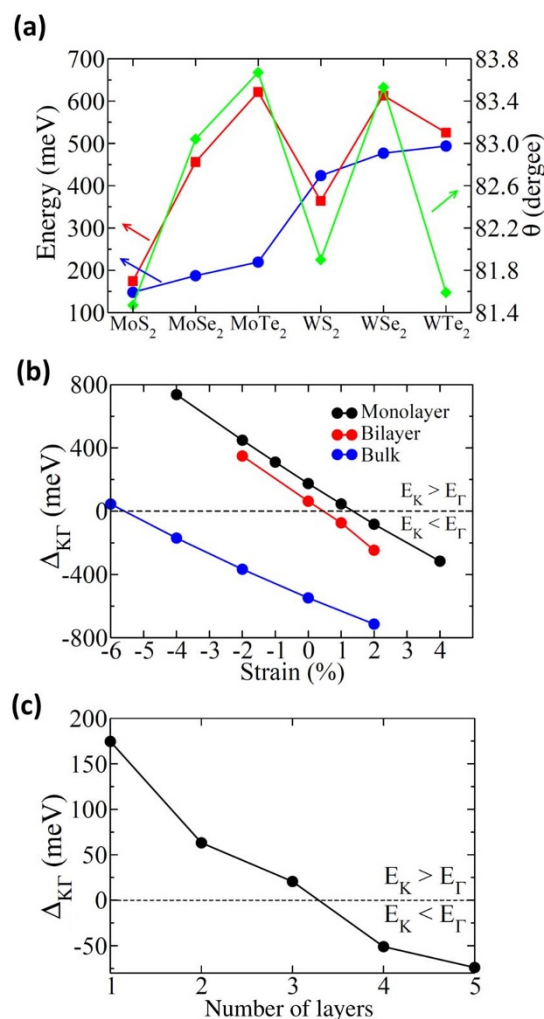

Figure 4 | (a) Spin-splitting energy Δ_{intra} (blue line), $\Delta_{K\Gamma}$ (red line) and X-M-X bond angle (green line) for various monolayer MX_2 materials. (b) $\Delta_{K\Gamma}$ as a function of in-plane strain in MoS_2. (c) $\Delta_{K\Gamma}$ as a function of slab thickness in MoS_2.

shown in Fig. 1(d), on the other hand, both the conduction minimum and valence bands maximum shift to the K-point, making a direct band gap. Our results are consistent with the fact that bulk MoS_2 has been demonstrated to support a large indirect-gap, which crosses over from indirect to a direct gap for a monolayer[20,21]. Such an indirect to direct band gap transition as the thickness is reduced has also been observed directly via ARPES spectroscopy for $MoSe_2$[46].

Conclusions

We have systematically investigated electronic structures of monolayer and bilayer films of transition-metal dichalcogenides MX_2 (M=Mo or W, X=S, Se, or Te) via first-principles calculations, and discuss how these electronic structures evolve in the bulk limit. In the monolayer case, the spin-splitting due to SOC occurs at the valence band maximum, resulting in two non-degenerate nearly 100% spin-polarized states with opposite out-of-the-plane polarizations at the K and K' symmetry points in the Brillouin zone. We show that the SOC induced spin splitting can be tuned by an out-of-the-plane external electric field for bilayer MX_2 thin films. Our theoretical results concerning the nature of the band gap, whether it is direct or indirect, and its evolution with layer thickness are in accord with recent experimental findings in several MX_2 materials. Our study provides insight into the degree of spin polarization of the

valence bands in ultra-thin transition-metal dichalcogenide films and their viability for spintronics applications.

1. Novoselov, K. S. *et al.* Electric Field Effect in Atomically Thin Carbon Films. *Science* **306**, 666 (2004).
2. Bolotin, K. I. *et al.* Ultrahigh electron mobility in suspended graphene. *Solid State Commun.* **146**, 351 (2008).
3. Novoselov, K. S. *et al.* Two-dimensional gas of massless Dirac fermions in graphene. *Nature* **438**, 197 (2005).
4. Zhang, Y., Tan, Y.-W., Stormer, H. L. & Kim, P. Experimental observation of the quantum Hall effect and Berry's phase in graphene. *Nature* **438**, 201 (2005).
5. Du, X., Skachko, I., Duerr, F., Luican, A. & Andrei, E. Y. Fractional quantum Hall effect and insulating phase of Dirac electrons in graphene. *Nature* **462**, 192 (2009).
6. Castro Neto, A. H., Guinea, F., Peres, M. R., Novoselov, K. S. & Geim, A. K. The electronic properties of graphene. *Rev. Mod. Phys.* **81**, 109 (2009).
7. König, M. *et al.* Quantum Spin Hall Insulator State in HgTe Quantum Wells. *Science* **318**, 766–770 (2007).
8. Bernevig, B. A., Hughes, T. L. & Zhang, S.-C. Quantum Spin Hall Effect and Topological Phase Transition in HgTe Quantum Wells. *Science* **314**, 1757–1761 (2006).
9. Vogt, R. *et al.* Silicene: Compelling Experimental Evidence for Graphenelike Two-Dimensional Silicon. *Phys. Rev. Lett.* **108**, 155501 (2012).
10. Coehoorn, R. *et al.* Electronic structure of $MoSe_2$, MoS_2, and WSe_2. I. Band-structure calculations and photoelectron spectroscopy. *Phys. Rev. B* **35**, 6195 (1987).
11. Dickinson, R. G. & Pauling, L. The Crystal structure of Molybdenite. *J. Am. Chem. Soc.* **45**, 1466 (1923).
12. Bronsema, K. D., de Boer, J. L. & Jellinek, F. On the structure of molybdenum diselenide and disulphide. *Z. Anorg. Alg. Chem.* **540/541**, 15 (1986).
13. Liu, C.-C., Feng, W. & Yao, Y. Quantum Spin Hall Effect in Silicene and Two-Dimensional Germanium. *Phys. Rev. Lett.* **107**, 076802 (2011).
14. Liu, C.-C., Jiang, H. & Yao, Y. Low-energy effective Hamiltonian involving spin-orbit coupling in silicene and two-dimensional germanium and tin. *Phys. Rev. B.* **84**, 195430 (2011).
15. Tsai, W.-F. *et al.* Gated silicene as a tunable source of nearly 100% spin-polarized electrons. *Nature Commun.* **4**, 1500 (2013).
16. Radisavljevic, B., Radenovic, A., Brivio, J., Giacometti, V. & Kis, A. Single-layer MoS_2 transistors. *Nature Nanotech.* **6**, 147 (2011).
17. Li, T. & Galli, G. Electronic Properties of MoS2 Nanoparticles. *J. Phys. Chem. C* **111**, 16192 (2007).
18. Lebegue, S. & Eriksson, O. Electronic structure of two-dimensional crystals from ab initio theory. *Phys. Rev. B* **79**, 115409 (2009).
19. Zhu, Z. Y., Cheng, Y. C. & Schwingenschlögl, U. Giant spin-orbit-induced spin splitting in two-dimensional transition-metal dichalcogenide semiconductors. *Phys. Rev. B* **84**, 153402 (2011).
20. Splendiani, A. *et al.* Emerging Photoluminescence in Monolayer MoS2. *Nano Lett.* **10**, 1271 (2010).
21. Mak, K. F., Lee, C., Hone, J., Shan, J. & Heinz, T. F. Atomically Thin MoS_2: A New Direct-Gap Semiconductor. *Phys. Rev. Lett.* **105**, 136805 (2010).
22. Zeng, H., Dai, J., Yao, W., Xiao, D. & Cui, X. Valley polarization in MoS_2 monolayers by optical pumping. *Nature Nanotech.* **7**, 490 (2012).
23. Mak, K. F., He, K., Shan, J. & Heinz, T. F. Control of valley polarization in monolayer MoS_2 by optical helicity. *Nature Nanotech.* **7**, 494 (2012).
24. Wu, S. *et al.* Electrical tuning of valley magnetic moment through symmetry control in bilayer MoS_2. *Nature Phy.* **9**, 149 (2013).
25. Cheng, Y. C., Zhu, Z. Y., Mi, W. B., Guo, Z. B. & Schwingenschlogl, U. Prediction of two-dimensional diluted magnetic semiconductors: Doped monolayer MoS_2 systems. *Phys. Rev. B* **87**, 100401(R) (2013).
26. Cheng, Y. C., Zhang, Q. Y. & Schwingenschlogl, U. Valley polarization in magnetically doped single-layer transition-metal dichalcogenides. *Phys. Rev. B* **89**, 155429 (2014).
27. Cheng, Y. C., Zhu, Z. Y. & Schwingenschlogl, U. Role of interlayer coupling in ultra thin MoS_2. *RSC Adv.* **2**, 7798 (2012).
28. Cheng, Y. C., Zhu, Z. Y., Tahir, M. & Schwingenschlogl, U. Spin-orbit induced spin splittings in polar transition metal dichalcogenide monolayers. *Europhys. Lett.* **102**, 57001 (2013).
29. Li, X., Zhang, F. & Niu, Q. Unconventional Quantum Hall Effect and Tunable Spin Hall Effect in Dirac Materials: Application to an Isolated MoS_2 Trilayer. *Phys. Rev. Lett.* **110**, 066803 (2013).
30. Ye, J. T. *et al.* Superconducting Dome in a Gate-Tuned Band Insulator. *Science* **38**, 1193 (2012).
31. Blöchl, P. E. Projector augmented-wave method. *Phys. Rev. B* **50**, 17953 (1994).
32. Kresse, G. & Joubert, J. From ultrasoft pseudopotentials to the projector augmented-wave method. *Phys. Rev. B* **59**, 1758 (1999).
33. Kress, G. & Hafner, J. Ab initio molecular dynamics for open-shell transition metals. *Phys. Rev. B.* **48**, 13115 (1993).
34. Kress, G. & Furthmüller, J. Efficiency of ab-initio total energy calculations for metals and semiconductors using a plane-wave basis set. *Comput. Mater. Sci.* **6**, 15 (1996).
35. Kress, G. & Furthmüller, J. Efficient iterative schemes for ab initio total-energy calculations using a plane-wave basis set. *Phys. Rev. B.* **54**, 11169 (1996).
36. Perdew, J. P., Burke, K. & Ernzerhof, M. Generalized Gradient Approximation Made Simple. *Phys. Rev. Lett.* **77**, 3865 (1996).
37. Dawson, W. G. & Bullett, D. W. Electronic structure and crystallography of $MoTe_2$ and WTe_2. *J. Phys. C: Solid State Phys.* **290**, 6159 (1987).
38. Bromley, R. A., Murray, R. B. & Yoffe, A. D. The band structures of some transition metal dichalcogenides. III. Group VIA: trigonal prism materials. *J. Phys. C* **5**, 759 (1972).
39. Feng, W. *et al.* K-edge x-ray absorption spectra in transition-metal oxides beyond the single-particle approximation: Shake-up many-body effects. *Phys. Rev. B* **86**, 165102 (2012).
40. Xio, D., Liu, G.-B., Feng, W., Xu, X. & YAo, W. Coupled Spin and Valley Physics in Monolayers of MoS_2 and Other Group-VI Dichalcogenides. *Phys. Rev. Lett.* **108**, 196802 (2012).
41. Zeng, H. *et al.* Optical signature of symmetry variations and spin-valley coupling in atomically thin tungsten dichalcogenides. *Sci. Rep.* **3**, 1608 (2013).
42. Gong, Z. *et al.* Magnetoelectric effects and valley-controlled spin quantum gates in transition metal dichalcogenide bilayers. *Nature Commun.* **4**, 2053 (2013).
43. Jones, A. M. *et al.* Spin-layer locking effects in optical orientation of exciton spin in bilayer WSe_2. *Nature Phys.* **10**, 130 (2014).
44. Sahrakorpi, S., Lindroos, M., Markiewicz, R. S. & Bansil, A. Evolution of Mid-gap States and Residual 3-Dimensionality in $La_{2-x}Sr_xCuO_4$. *Phys. Rev. Lett.* **95**, 157601 (2005).
45. Alfredsson, M. *et al.* Structural and magnetic phase transitions in simple oxides using hybrid functionals. *Mol. Simulat.* **31**, 367 (2005).
46. Zhang, Y. *et al.* Direct observation of the transition from indirect to direct bandgap in atomically thin epitaxial $MoSe_2$. *Nature Nanotech.* **9**, 111 (2014).

Acknowledgments

Author contributions

T.-R.C. performed the calculations. T.-R.C., H.L., H.-T.J. and A.B. prepared the manuscript.

Additional information